

Bidirectional Modulation of Contact Thermal Resistance between Boron Nitride Nanotubes from a Polymer Interlayer

Zhiliang Pan, Yi Tao, Yang Zhao, Matthew L. Fitzgerald, James R. McBride, Lei Zhu, and Deyu Li*

Cite This: *Nano Lett.* 2021, 21, 7317–7324

Read Online

ACCESS |

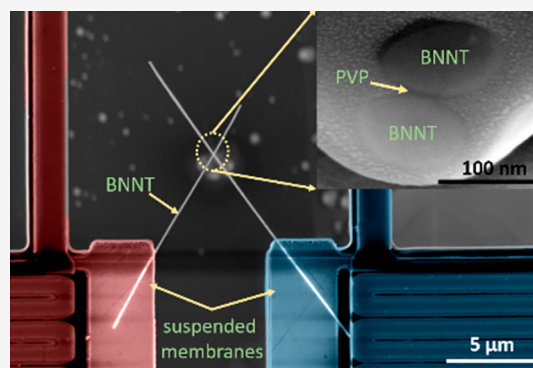
Metrics & More

Article Recommendations

Supporting Information

ABSTRACT: Enhancing the thermal conductivity of polymer composites could improve their performance in applications requiring fast heat dissipation. While significant progress has been made, a long-standing issue is the contact thermal resistance between the nanofillers, which could play a critical role in the composite thermal properties. Through systematic studies of contact thermal resistance between individual boron nitride nanotubes (BNNTs) of different diameters, with and without a poly(vinylpyrrolidone) (PVP) interlayer, we show that the contact thermal resistance between bare BNNTs is largely determined by reflection of ballistic phonons. Interestingly, it is found that a PVP interlayer can either enhance or reduce the contact thermal resistance, as a result of converting the ballistic phonon dominated transport into diffusion through the PVP layer. These results disclose a previously unrecognized physical picture of thermal transport at the contact between BNNTs, which provides insights into the design of high thermal conductivity BNNT–polymer composites.

KEYWORDS: Phonon transport, polymer composites, boron nitride nanotubes, thermal conductivity, thermal conductivity enhancement



Thermally conductive polymer composites are of current interest for various applications that require rapid heat dissipation.^{1–3} Various filler materials, including carbon nanotubes (CNTs),^{4–6} ceramic particles,^{7–9} and metal nanowires,^{10–13} have been tested for enhancing composite thermal conductivity. For applications as thermal interface materials in electronic/optoelectronic devices and as structural materials mounted with high power devices, it is highly desirable to have thermally conductive yet electrically insulating composites.¹⁴ Toward this goal, boron nitride nanotubes and nanosheets have been identified as promising filler materials to enhance the thermal conductivity of polymer composites without jeopardizing their electrical insulation properties.^{14–16} While significant progress has been made, issues related to the contact thermal resistance between these nanofillers remain poorly understood.

Given the experimental challenge of directly measuring contact thermal resistance between nanostructures, traditionally its values have been inferred from the measured thermal conductivity of bulk composites using various effective media models.³ The values from different studies often vary drastically and do not match well with expectations.^{3,17,18} Meanwhile, limited efforts on directly measuring contact thermal resistance between nanofillers have disclosed unusual observations, such as the diameter dependent contact thermal conductance per unit area between multiwalled CNTs (MWCNTs),¹⁹ which was previously regarded as size independent. In addition, one interesting question is the effect

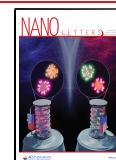
of a polymer interlayer on the contact thermal resistance as it often presents at the contact between nanofillers. Through systematic studies of the thermal resistance of the contacts between individual BNNTs with and without a PVP interlayer, here we report on the unexpected bidirectional modulation of the contact thermal resistance by a PVP interlayer.

To measure the contact thermal resistance, BNNT suspension obtained via sonication of BNNT powder (Nano-Integris Technologies) was first drop-casted onto a piece of polydimethylsiloxane (PDMS). Using a sharp probe mounted on a micromanipulator, an individual BNNT was broken into two segments, which were then transferred to the measurement device to form a contact sample for thermal measurement,^{20–22} as shown in the scanning electron microscopy (SEM) image in Figure 1a. Afterward, one segment was realigned between the heat source and heat sink (Figure 1b) for measuring the resistance of the single continuous tube. Comparison of these two measurement results allows for extraction of the thermal resistance of point contacts between bare BNNTs.

Received: June 27, 2021

Revised: August 17, 2021

Published: August 20, 2021



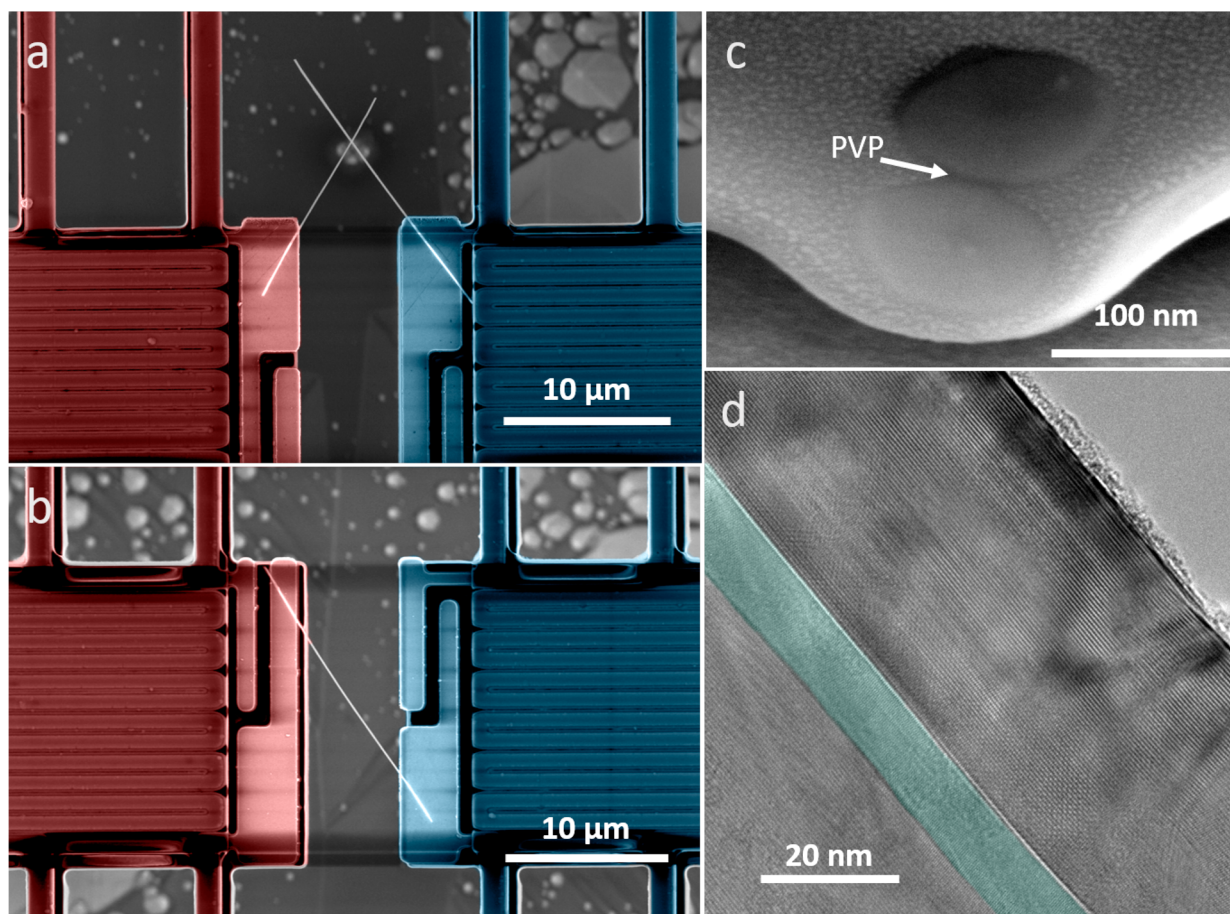


Figure 1. SEM micrographs of (a) a contact sample and (b) a single tube segment on the measurement devices. The diameter of this BNNT is 102 nm and special care has been taken to guarantee the total suspended tube length for heat conduction between the two membranes to be approximately the same. (c) SEM micrograph showing the cross-section of the contact with a PVP interlayer for the 102 nm diameter BNNTs post the thermal measurement. The image was captured at a tilted angle of 38° between the electron beam and the surface normal. (d) TEM micrograph of the 102 nm diameter BNNT. The tube layer can be clearly identified and the wall thickness is extracted from the image. The center hollow region is highlighted with green color.

Table 1. Sample Geometry Information^a

sample ID	D (nm)	t_{wall} (nm)	β (deg)	A (nm ²)	L_s (μm)	$L_{\text{c_tot}}$ (μm)	$L_{\text{cp_tot}}$ (μm)	t_{PVP} (nm)
C1	102	43.0	65.5	230.1	11.9	11.7	12.0	13.1
C2	92	37.0	73.0	189.2	10.4	10.2	10.4	13.0
C3	80	32.0	80.1	154.5	9.3	9.3	9.5	12.5
C4	74	31.0	89.0	135.3	11.8	11.6	11.7	13.0
C5	62	25.0	80.0	104.4		10.5	10.3	13.4
C6	67	28.5	97.5	115.8	12.3	12.6		
C7	62	25.0	85.7	109.9	13.4	13.6		
C8	51	20.5	88.2	78.5	9.1	9.2		
C9	47	19.5	77.5	71.5	14.4	14.8		

^a D is the BNNT outer diameter. β and A are the contact angle and contact area, respectively. L_s is the suspended length of the single continuous tube. $L_{\text{cp_tot}}$ and $L_{\text{c_tot}}$ are the combined suspended lengths of two segments in the contact samples with and without a PVP interlayer, respectively. t_{wall} and t_{PVP} denote BNNT wall thickness and PVP interlayer thickness, respectively. Note that t_{PVP} can be extracted by either comparing the tube diameter change before and after PVP coating or measuring the polymer thickness from the cross-section image. The values from these two different approaches match each other well (13.3 nm/13.1 nm for the 102 nm sample).

For measurements of the contact thermal resistance with a PVP interlayer between BNNTs, PVP powder (Sigma-Aldrich, 437190-25G, molecular weight = 1300 kg mol⁻¹) was dissolved in ethanol (Sigma-Aldrich, 187380-1L) at a ratio of 1:10 (w/w) and drop-cast onto a piece of PDMS. One BNNT segment was picked up with the probe and dipped into the PVP solution for a few seconds. The BNNT was then pulled

out of the PVP solution and left in the air for ~20 min, which allowed for the ethanol to evaporate, resulting in a BNNT with a portion coated with a thin layer of PVP, as identified in the Supporting Information (section I). This BNNT segment was then aligned with the other bare BNNT segment to form a contact sample with a PVP interlayer between the BNNTs,

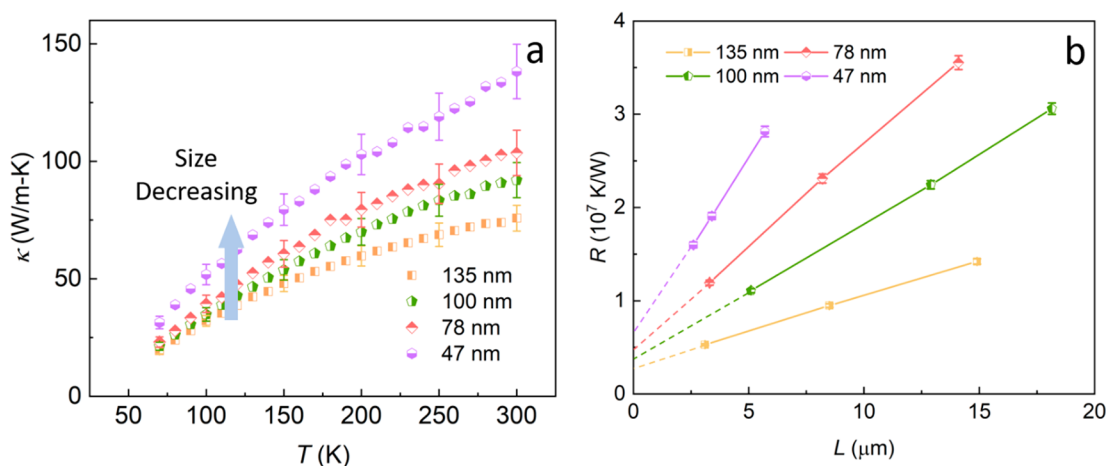


Figure 2. Thermal property of BNNTs. (a) Intrinsic thermal conductivity of different diameter BNNTs. Data were extracted through fitting the resistance-length curves from panel b.²³ The extracted intrinsic thermal conductivity increases as the tube size reduces. (b) Measured thermal resistance versus sample length at 300 K for continuous tubes.

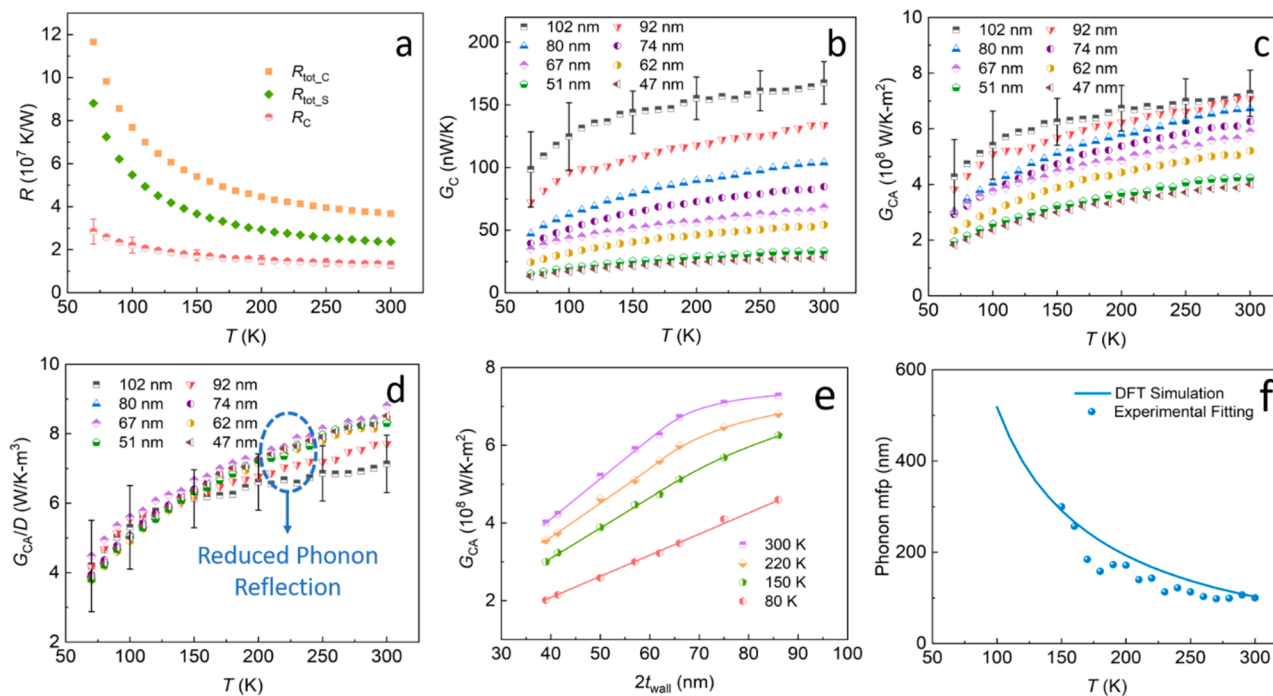


Figure 3. Contact thermal resistance between bare BNNTs. (a) Thermal resistance components of a 74 nm diameter sample. (b) Contact thermal conductance, G_C , between bare BNNTs. G_C shows a clear size dependence. (c) Contact thermal conductance per unit area, G_{CA} , between bare BNNTs. G_{CA} still increases with tube size. (d) G_{CA} normalized by D . Data for the 92 and 102 nm diameter samples deviate from the others at elevated temperatures above 150 K. (e) G_{CA} versus the doubled wall thickness. While G_{CA} increases linearly with the wall thickness in the low temperature regime, the increasing trend gets flatter as the wall thickness increases beyond 150 K. (f) Extracted cross-plane phonon mfp from fitting the experimental data and DFT simulations.

allowing for measurements of the BNNT–PVP–BNNT contact.

An SEM micrograph of the contact region between the two 102 nm diameter BNNTs is shown in Figure 1c, where a ~ 13 nm thick PVP layer between the two BNNTs can be clearly identified. Figure 1d illustrates a transmission electron microscopy (TEM) micrograph of the layered structure of the same sample. We note that analysis of the TEM images of all measured BNNTs indicates that the BNNT wall thickness is approximately proportional to the tube diameter, as listed in Table 1.

The measured total thermal resistance of the single continuous tube (R_{tot_S}) and the contact sample (R_{tot_C}) can be written as

$$R_{\text{tot}_S} = R_{C,M} + R_{w,s} \quad (1)$$

$$R_{\text{tot}_C} = R_{C,M} + R_{w,c} + R_C \quad (2)$$

Here, $R_{C,M}$ is the contact thermal resistance between the sample and the two suspended membranes, while $R_{w,s}$ and $R_{w,c}$ represent the intrinsic thermal resistance of the suspended BNNT segments for the single tube and the contact sample, respectively. R_C is the contact resistance between the two

BNNTs. Significant efforts have been made to guarantee that the length of the suspended BNNTs for heat conduction between the two membranes in the single tube and the contact sample are approximately the same, with a maximum difference of only 2.5% (see Table 1). Therefore, it is reasonable to assume that $R_{w,s}$ and $R_{w,c}$ are approximately the same and can be canceled out in solving for R_C through subtracting eq 1 from eq 2, that is, $R_C = R_{tot_C} - R_{tot_S}$.

Note that for the above derivation to be valid, $R_{C,M}$ needs to remain constant between measurements for the same BNNT sample, which is indeed the case as suggested by the linear profile between the measured resistance and the sample length in Figure 2b. In addition, an analysis of $R_{C,M}$ indicates that the thermalization distance,^{23,24} that is, the contact length required for the tube to reach thermal equilibrium with the membranes, is below 2 μm for all BNNTs. The minimum contact length for all samples is $\sim 2.5 \mu\text{m}$, which satisfies the requirement for $R_{C,M}$ to remain the same for the continuous tube and contact sample (section II in the Supporting Information).

Four BNNTs were measured to evaluate the intrinsic thermal conductivity of individual tubes. For each sample, the thermal conductance for three different suspended lengths were measured following an approach used to extract the intrinsic thermal conductivity (κ) of MWCNTs.²³ Figure 2a indicates that κ increases as the tube diameter reduces, which is a common trend for CNTs and BNNTs as the structural quality is usually better for thinner tubes.²⁵

Importantly, the linear profile with the suspended length above 3 μm in Figure 2b indicates fully diffusive phonon transport in the tube beyond this length scale. The shortest BNNT segment in the following contact resistance measurements is $\sim 3.8 \mu\text{m}$, and therefore, no complication from ballistic phonon transport is involved when comparing $R_{w,s}$ and $R_{w,c}$. In addition, $R_{C,M}$ can be extracted from the plot of measured total thermal resistance versus sample length (Figure 2b) as the intercept with the vertical axis, and the weight of $R_{C,M}$ is always less than 15% of R_{tot_S} and R_{tot_C} .

Next, R_C between bare BNNTs was measured for eight samples of different diameters, as listed in Table 1. The tube length was obtained from SEM examination while the tube diameter and wall thickness were extracted via TEM studies. Figure 3a shows extracted R_{tot_C} , R_{tot_S} , and R_C for a 74 nm sample. At room temperature, R_C contributes $\sim 35\%$ to R_{tot_C} well beyond the measurement uncertainty (section III in the Supporting Information).

Figure 3b plots the extracted contact thermal conductance, G_C , which increases monotonically with the tube diameter. To further understand the phonon transport mechanism at the tube–tube contact, we solve for contact thermal conductance per unit area, G_{CA} . To do so, we calculated the contact area using the Maugis model,^{19,26} as listed in Table 1. As shown in Figure 3c, G_{CA} , which is normally size-independent, still increases with the tube diameter, indicating more interesting transport physics at the contact. Similar phenomenon has been observed for MWCNTs,¹⁹ which is explained based on three coupled mechanisms. First, the phonon mean free path (mfp) along the radial direction of the tube in MWCNTs is ~ 200 nm, well-beyond the traditionally believed value. This renders ballistic transport of phonons through the contact, which can be reflected by the innermost layer of the receiving tube back into the emitting tube, and do not contribute to thermal transport from one tube to the other. Only when phonons experience scattering in the receiving tube, they deliver energy

across the contact and contribute to G_C . Since the possibility of phonons getting thermalized when they travel in the receiving tube is proportional to the wall thickness, and hence the tube diameter, G_{CA} becomes a function of diameter. Note that for the above picture to be valid, phonons responsible for G_C need to transport largely along the tube radial direction, which is indeed the case considering the phonon focusing effect induced by the drastically different bonding strengths within each tube layer and between different tube layers.

Similar physical picture can be applied to contacts between BNNTs and to verify this, G_{CA}/D , where D is the tube diameter, is plotted in Figure 3d. It can be seen that the G_{CA}/D curves for different diameter samples overlap with each other, except for the 92 and 102 nm samples at elevated temperatures. At room temperature, G_{CA}/D for the 102 nm sample is 16% lower than the average value for the six thinner samples, which is beyond the measurement uncertainty. This deviation can be explained by the fact that as temperature increases, the phonon mfp gets shorter and becomes comparable to $2t_{wall}$, where t_{wall} is the wall thickness.

It has been shown that the phonon mfp along the c -axis for graphite and MoS_2 could be well over 100 nm;^{27–29} however, no such data have been reported for boron nitride. As such, we estimate the phonon mfp for boron nitride based on the diameter dependence of G_{CA} . Figure 3e plots G_{CA} as a function of the doubled wall thickness ($2t_{wall}$) at different temperatures, and a linear trend can be clearly observed at 80 K. Above 150 K, the increasing trend of G_{CA} becomes flatter as $2t_{wall}$ increases beyond ~ 66 nm, indicating that the phonon mfp above 150 K along the c -axis of boron nitride should be comparable to this value.

A model can be constructed to extract the cross-plane phonon mfp. The probability of a phonon traveling over a distance ΔL along the radial direction without being scattered can be written as $P = e^{-\Delta L/\lambda}$,³⁰ where λ is the phonon mfp. Considering that phonons will be reflected at the innermost layer and travel through the tube wall twice, the energy absorbed (E_a) by the receiving tube is related to the incoming energy (E_i) carried by phonons from the other tube as

$$E_a = (1 - e^{-2t_{wall}/\lambda})E_i \quad (3)$$

The effective phonon transmission probability across the contact, α , as a result of phonon reflection at the innermost layer, can then be written as

$$\alpha = \frac{E_a}{E_i} = 1 - e^{-2t_{wall}/\lambda} \quad (4)$$

Note that since λ depends on temperature so α is also a function of temperature. This leads to the following relation

$$G_{CA}(T) = (1 - e^{-2t_{wall}/\lambda})G_{CA,0} \quad (5)$$

where $G_{CA,0}$ is the contact thermal conductance per unit area without the effect of phonon reflection. Through fitting the experimental data set of G_{CA} versus $2t_{wall}$, λ and $G_{CA,0}$ can be extracted. The resulting phonon mfp is shown in Figure 3f. At 300 K, λ is ~ 100 nm, while at 150 K, λ increases to 300 nm. This observation is consistent with the findings that the phonon mfp along the c -axis of graphite and MoS_2 is on the order of 100 nm, much longer than the traditionally believed value of just a few nanometers.^{31,32}

To further verify this result, density functional theory (DFT) based calculations were performed on bulk BN, which was

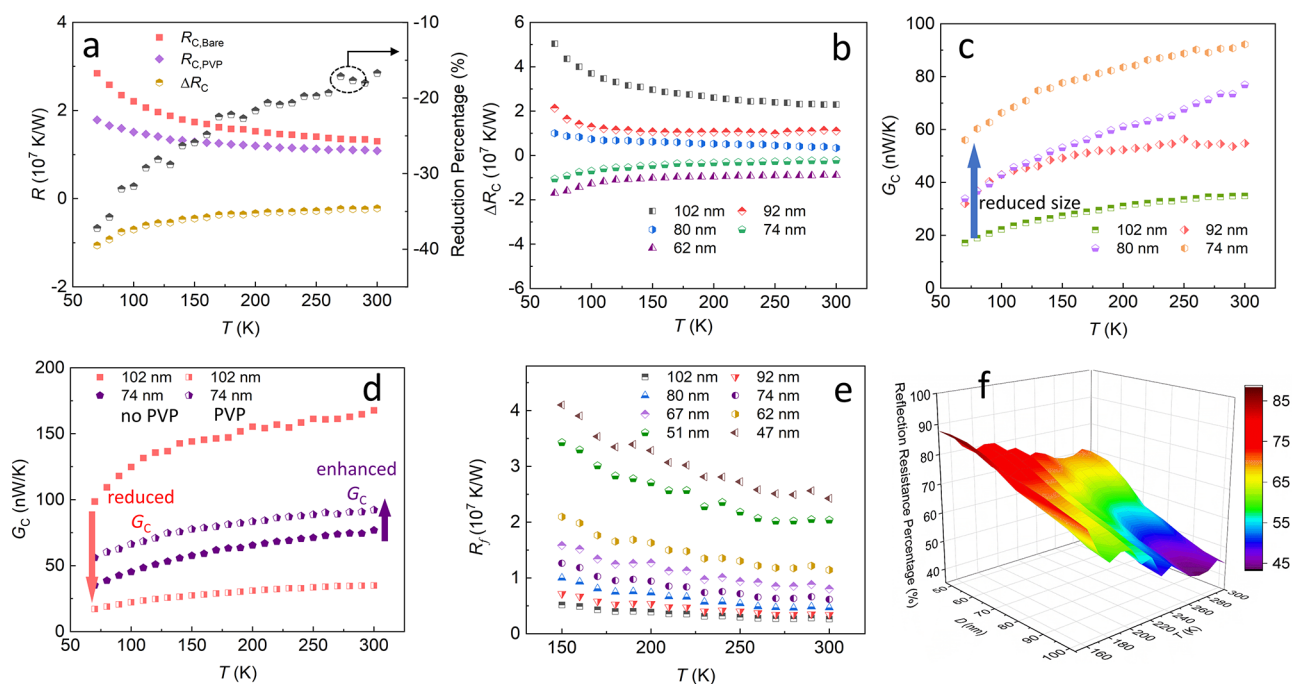


Figure 4. (a) Contact thermal resistance for the 74 nm diameter sample with and without a PVP layer (left axis), and the percentage reduction with the PVP layer is also shown (right axis). ΔR_C is the contact thermal resistance difference with and without PVP layer. Surprisingly, R_C becomes smaller with the PVP interlayer. (b) ΔR_C for samples of different sizes. (c) G_C with the PVP layer as a function of the tube size. Counterintuitively, as size reduces, G_C increases, opposite to the trend for bare tube contacts. (d) Bidirectional modulation of G_C by the PVP layer. With the PVP interlayer, G_C decreases for the 102 nm diameter sample and increases for the 74 nm diameter sample. (e) Contact thermal resistance induced by phonon reflection, R_f , for contacts between bare tubes. R_f increases rapidly as the tube size reduces. (f) Contribution of R_f to R_C . The percentage contribution from R_f increases as the temperature and tube diameter reduce.

based on the Vienna ab initio simulation package (VASP).³³ An energy cutoff of 520 eV was chosen for the plane wave basis sets in the projector augmented wave (PAW) method.³⁴ The exchange correlation interaction was treated with the general gradient approximation (GGA) in the Perdew–Burke–Ernzerhof (PBE) parametrization considering the vdW correction.^{35,36} The phonon mfp was obtained by solving the phonon Boltzmann transport equation (BTE) under the relaxation time approximation as implemented in the Sheng BTE code.³⁷ As shown in Figure 3f, the simulation fits the extracted cross-plane phonon mfp from the experimental data reasonably well. The slightly lower values derived from the experimental data could be because of the imperfections involved in the sample quality, such as defects in the tubes and the surface residues at the contact.

To explore the effect of a thin polymer interlayer on the contact thermal resistance, five samples with a BNNT–PVP–BNNT contact morphology have been measured. The thickness of the PVP layer is ~ 13 nm for all five samples. Figure 4a shows the extracted R_C for the 74 nm tube with and without the PVP layer. Interestingly, contrary to the expectation that the PVP layer will add additional resistance and increase R_C , it actually leads to a lower R_C . It is worth noting that the reduction percentage increases as temperature drops. More interestingly, results in Figure 4b (and Figure S3) suggest that the contact resistance change ΔR_C ($\Delta R_C = R_{C,PVP} - R_{C,Bare}$, where $R_{C,PVP}$ and $R_{C,Bare}$ are contact thermal resistance with and without the PVP layer, respectively) is positive for larger tubes and negative for smaller tubes, which means that the PVP interlayer increases R_C for the 80, 92, 102 nm diameter tubes but reduces the corresponding value for the 62 and 74 nm diameter tubes. This observation illustrates a

bidirectional modulation of G_C by the PVP interlayer. In fact, with the PVP interlayer, G_C presents an opposite size dependence compared to the case for bare tubes (Figure 4c); and for the 102 nm diameter sample, after introducing a PVP interlayer, G_C is greatly reduced, while for the 74 nm diameter sample, G_C is enhanced (Figure 4d).

The bidirectional modulation of R_C indicates competing effects of the PVP interlayer on R_C . On one hand, the PVP interlayer introduces additional thermal resistance as it is of very low thermal conductivity (~ 0.23 W/m-K at 300 K);³⁸ on the other hand, the effective contact area between the BNNTs is enlarged by the PVP interlayer. While it seems that these two competing mechanisms could be responsible for the opposite trends of the contact thermal resistance between BNNTs of large and small diameters, in-depth analysis discloses more interesting physical picture behind the observation.

First, the enhancement of R_C for larger diameter tubes cannot be simply regarded as the additional thermal resistance of the PVP. For the 80 nm diameter tube, for example, ΔR_C at 300 K is only 3.4×10^6 K/W. If this resistance change is treated as that of the PVP layer, it can be calculated as $\Delta R_C = t_{PVP}/\kappa_{PVP}A_C$, where t_{PVP} and κ_{PVP} are the thickness and thermal conductivity of the PVP layer, respectively, and A_C is the contact area. Taking t_{PVP} as 12.5 nm and κ_{PVP} as 0.23 W/m-K, the resulting A_C is $16\,105$ nm², which corresponds to a diameter of 143.2 nm if the contact is assumed to be a circle. This dimension is beyond the tube diameter so treating ΔR_C as the additional resistance from the PVP interlayer is not reasonable.

In fact, the PVP interlayer fundamentally altered the phonon transport picture at the contact. For contacts between bare BNNTs, phonons from the emitting tube can ballistically

transmit through the contact and G_{CA} is largely determined by whether these phonons can be thermalized in the receiving tube or, equivalently, to what extent these phonons are reflected back into the emitting tube determines R_C . However, the PVP interlayer disrupts this ballistic transport as phonons can only diffuse through the PVP layer. In fact, it has been shown that a nanometer thick organic residual layer between two boron nanoribbons can completely eliminate the ballistic transmission of phonons through the van der Waals interface between the two ribbons.³⁹ In this case, the PVP interlayer largely determines the contact thermal resistance. This is the case for the larger tubes when phonon reflection is not the dominant factor for R_C because of the large t_{wall} . As shown in Figure 4d, for the 102 nm diameter sample, $G_{C,Bare}$ is much larger than $G_{C,PVP}$. The reduction is primarily caused by the resistance of the PVP layer. However, as the tube size reduces, phonon reflection contributes more to $R_{C,Bare}$. As shown in Figure 4e, phonon reflection induced thermal resistance R_f ($R_f = R_{C,Bare} - 1/AG_{CA,0}$) increases dramatically as the tube size reduces. Figure 4f plots the contribution of R_f to R_C as the tube diameter and temperature changes, which indicates that phonon reflection contributes $\sim 44\%$ to R_C for the 102 nm sample and it increases to $\sim 71\%$ for the 47 nm diameter sample at room temperature. At low temperatures, R_f contributes even more.

As discussed above, the additional PVP layer can eliminate the ballistic transmission of phonons thus remove R_f from R_C at the cost of introducing the interfacial resistance ($R_{interface}$) and polymer resistance (R_{PVP}). The net effect, ΔR_C , follows $\Delta R_C = R_{PVP} + R_{interface} - R_f$. For larger tubes, R_f is small compared to $R_{PVP} + R_{interface}$, hence ΔR_C is positive. As size reduces, R_f increases, and ΔR_C reduces and eventually becomes negative. This can also explain the temperature dependence of the relative resistance reduction in Figure 4a. At low temperatures, phonon mfp increases, leading to a much larger R_f while resistance posed by PVP does not increase as much. Thus, the reduction is more pronounced.

In polymer composites, direct filler–filler contacts have usually been considered beneficial for thermal transport by reducing R_C and forming a percolated filler thermal pathway.^{18,40–42} However, for highly anisotropic materials like CNTs and BNNTs, as a result of phonon reflection, R_C between tubes could be comparable to interfacial resistance ($1\text{--}2 \times 10^{-9} \text{ m}^2 \text{ K/W}$ for BN based composites)^{43,44} and be equivalent to the resistance of a polymer layer of a few tens of nanometers thick, which could render more than 1 order of magnitude reduction in thermal conductivity for CNT network.^{19,45–48} In this case, a thin polymer layer between CNTs or BNNTs could actually reduce the contact thermal resistance and result in a more thermally conductive filler thermal pathway. This is especially true for BNNT-based composites, as $R_{interface}$ between BNNTs and polymer matrices is believed to be lower than that between CNTs and polymers.^{49–52}

In summary, this study discloses interesting observation of contact thermal resistance between bare BNNTs and bidirectional modulation of the contact resistance from a PVP interlayer. Analysis indicates that these results are due to conversion from ballistic phonon transmission and back reflection for contacts between bare BNNTs to diffusive transport through a PVP interlayer. These previously unrecognized phenomena and understandings provide important

insights into better tuning the thermal properties of BNNT–polymer composites for different applications.

METHODS

Thermal Transport Property Measurements. The thermal measurements were conducted in a cryostat ((Janis CCS-400/204) under a high vacuum ($<1 \times 10^{-6}$ mbar). Dual radiation shields were used to minimize the effects of radiation. The measurements were conducted following a well-established procedure.^{21–23} A Wheatstone bridge setup was adopted at the sensing side of the device to improve measurement sensitivity,²² which allows for a measurement resolution of ~ 0.1 nW/K at room temperature based on the settings for measurements in this study.

Microscopy. SEM examination is conducted with either a Zeiss Merlin SEM with a GEMINI II column or the integrated SEM in a dual beam FEI Helios NanoLab G3 CX FIB-SEM. TEM studies are done using an FEI Tecnai G2 Osiris S/TEM. The cross-section of the contact is obtained through first depositing a Pt/C coating using electron beam induced deposition and then cutting at different locations with the focused ion beam, following a procedure in previous reports.^{53,54}

ASSOCIATED CONTENT

Supporting Information

The Supporting Information is available free of charge at <https://pubs.acs.org/doi/10.1021/acs.nanolett.1c02504>.

Sample preparation and characterization, contact thermal resistance analysis, experimental uncertainty, size dependence of ΔR_C at different temperatures, and additional information on DFT simulation (PDF)

AUTHOR INFORMATION

Corresponding Author

Deyu Li – Department of Mechanical Engineering, Vanderbilt University, Nashville, Tennessee 37235, United States; orcid.org/0000-0001-8364-0924; Email: deyu.li@vanderbilt.edu

Authors

Zhiliang Pan – Department of Mechanical Engineering, Vanderbilt University, Nashville, Tennessee 37235, United States; orcid.org/0000-0002-6154-2765

Yi Tao – Department of Mechanical Engineering, Vanderbilt University, Nashville, Tennessee 37235, United States; School of Mechanical Engineering and Jiangsu Key Laboratory for Design and Manufacture of Micro-Nano Biomedical Instruments, Southeast University, Nanjing 210096, P. R. China

Yang Zhao – Department of Mechanical Engineering, Vanderbilt University, Nashville, Tennessee 37235, United States

Matthew L. Fitzgerald – Department of Mechanical Engineering, Vanderbilt University, Nashville, Tennessee 37235, United States; orcid.org/0000-0002-9103-2328

James R. McBride – Department of Chemistry, The Vanderbilt Institute of Nanoscale Science and Engineering, Vanderbilt University, Nashville, Tennessee 37235, United States; orcid.org/0000-0003-0161-7283

Lei Zhu – Department of Macromolecular Science and Engineering, Case Western Reserve University, Cleveland,

Ohio 44106, United States; orcid.org/0000-0001-6570-9123

Complete contact information is available at:
<https://pubs.acs.org/10.1021/acs.nanolett.1c02504>

Author Contributions

Z.P., M.L.F., and Y.Z. prepared PVP-coated samples. Z.P. performed the thermal measurements. Y.T. conducted DFT simulations. Z.P. and D.L. analyzed data and wrote the manuscript. Z.P. and J.M. conducted the TEM examination. Z.L. and D.L. supervised the project. All authors discussed the results and commented on the manuscript.

Notes

The authors declare no competing financial interest.

ACKNOWLEDGMENTS

The authors thank the financial support from the U.S. National Science foundation (Awards 1903645 and 1532107). M.L.F. acknowledges the graduate fellowship support from the National Aeronautics and Space Administration (NSTRF18_80NSSC18K1165). Y.T. acknowledges financial support from the China Scholarship Council (CSC No. 201806090027). This work was performed in part at the Cornell NanoScale Facility, an NNCI member supported by NSF Grant NNCI-2025233.

REFERENCES

- (1) Pop, E. Energy dissipation and transport in nanoscale devices. *Nano Res.* **2010**, *3* (3), 147–169.
- (2) Moore, A. L.; Shi, L. Emerging challenges and materials for thermal management of electronics. *Mater. Today* **2014**, *17* (4), 163–174.
- (3) Xu, X.; Chen, J.; Zhou, J.; Li, B. Thermal conductivity of polymers and their nanocomposites. *Adv. Mater.* **2018**, *30* (17), 1705544.
- (4) Guthy, C.; Du, F.; Brand, S.; Winey, K. I.; Fischer, J. E. Thermal Conductivity of Single-Walled Carbon Nanotube/PMMA Nanocomposites. *J. Heat Transfer* **2007**, *129* (8), 1096–1099.
- (5) King, J. A.; Lopez Gaxiola, D.; Johnson, B. A.; Keith, J. M. Thermal conductivity of carbon-filled polypropylene-based resins. *J. Compos. Mater.* **2010**, *44* (7), 839–855.
- (6) Song, Y. S.; Youn, J. R. Influence of dispersion states of carbon nanotubes on physical properties of epoxy nanocomposites. *Carbon* **2005**, *43* (7), 1378–1385.
- (7) Zhou, T.; Wang, X.; Gu, M.; Liu, X. Study of the thermal conduction mechanism of nano-SiC/DGEBA/EMI-2,4 composites. *Polymer* **2008**, *49* (21), 4666–4672.
- (8) Yu, S.; Hing, P.; Hu, X. Thermal conductivity of polystyrene–aluminum nitride composite. *Composites, Part A* **2002**, *33* (2), 289–292.
- (9) Gu, J.; Zhang, Q.; Dang, J.; Zhang, J.; Yang, Z. Thermal conductivity and mechanical properties of aluminum nitride filled linear low-density polyethylene composites. *Polym. Eng. Sci.* **2009**, *49* (5), 1030–1034.
- (10) Xu, J.; Munari, A.; Dalton, E.; Mathewson, A.; Razeeb, K. M. Silver Nanowire Array-Polymer Composite as Thermal Interface Material. *J. Appl. Phys.* **2009**, *106*, 124310.
- (11) Wang, S.; Cheng, Y.; Wang, R.; Sun, J.; Gao, L. Highly Thermal Conductive Copper Nanowire Composites with Ultralow Loading: Toward Applications as Thermal Interface Materials. *ACS Appl. Mater. Interfaces* **2014**, *6* (9), 6481–6486.
- (12) Boudenne, A.; Ibos, L.; Fois, M.; Majeste, J. C.; Gehin, E. Electrical and thermal behavior of polypropylene filled with copper particles. *Composites, Part A* **2005**, *36* (11), 1545–1554.
- (13) Balachander, N.; Seshadri, I.; Mehta, R. J.; Schadler, L. S.; Borca-Tasciuc, T.; Koblinski, P.; Ramanath, G. Nanowire-Filled

Polymer Composites with Ultrahigh Thermal Conductivity. *Appl. Phys. Lett.* **2013**, *102*, No. 093117.

(14) Zhi, C.; Bando, Y.; Terao, T.; Tang, C.; Kuwahara, H.; Golberg, D. Towards thermoconductive, electrically insulating polymeric composites with boron nitride nanotubes as fillers. *Adv. Funct. Mater.* **2009**, *19* (12), 1857–1862.

(15) Terao, T.; Bando, Y.; Mitome, M.; Zhi, C.; Tang, C.; Golberg, D. Thermal conductivity improvement of polymer films by catechin-modified boron nitride nanotubes. *J. Phys. Chem. C* **2009**, *113* (31), 13605–13609.

(16) Yang, X.; Guo, Y.; Han, Y.; Li, Y.; Ma, T.; Chen, M.; Kong, J.; Zhu, J.; Gu, J. Significant improvement of thermal conductivities for BNNS/PVA composite films via electrospinning followed by hot-pressing technology. *Composites, Part B* **2019**, *175*, 107070.

(17) Chen, H.; Ginzburg, V. V.; Yang, J.; Yang, Y.; Liu, W.; Huang, Y.; Du, L.; Chen, B. Thermal conductivity of polymer-based composites: Fundamentals and applications. *Prog. Polym. Sci.* **2016**, *59*, 41–85.

(18) Han, Z.; Fina, A. Thermal conductivity of carbon nanotubes and their polymer nanocomposites: A review. *Prog. Polym. Sci.* **2011**, *36* (7), 914–944.

(19) Yang, J.; Shen, M.; Yang, Y.; Evans, W. J.; Wei, Z.; Chen, W.; Zinn, A. A.; Chen, Y.; Prasher, R.; Xu, T. T.; Koblinski, P.; Li, D. Phonon transport through point contacts between graphitic nanomaterials. *Phys. Rev. Lett.* **2014**, *112* (20), 205901.

(20) Shi, L.; Li, D.; Yu, C.; Jang, W.; Kim, D.; Yao, Z.; Kim, P.; Majumdar, A. Measuring Thermal and Thermoelectric Properties of One-Dimensional Nanostructures Using a Microfabricated Device. *J. Heat Transfer* **2003**, *125* (5), 881–888.

(21) Wingert, M. C.; Chen, Z. C. Y.; Kwon, S.; Xiang, J.; Chen, R. Ultra-Sensitive Thermal Conductance Measurement of One-Dimensional Nanostructures Enhanced by Differential Bridge. *Rev. Sci. Instrum.* **2012**, *83* (2), No. 024901.

(22) Yang, L.; Yang, Y.; Zhang, Q.; Zhang, Y.; Jiang, Y.; Guan, Z.; Gerboth, M.; Yang, J.; Chen, Y.; Walker, D. G.; Xu, T. T.; Li, D. Thermal conductivity of individual silicon nanoribbons. *Nanoscale* **2016**, *8* (41), 17895–17901.

(23) Yang, J.; Yang, Y.; Waltermire, S. W.; Gutu, T.; Zinn, A. A.; Xu, T. T.; Chen, Y.; Li, D. Measurement of the intrinsic thermal conductivity of a multiwalled carbon nanotube and its contact thermal resistance with the substrate. *Small* **2011**, *7* (16), 2334–2340.

(24) Yu, C.; Saha, S.; Zhou, J.; Shi, L.; Cassell, A. M.; Cruden, B. A.; Ngo, Q.; Li, J. Thermal contact resistance and thermal conductivity of a carbon nanofiber. *J. Heat Transfer* **2006**, *128* (3), 234–239.

(25) Pettes, M. T.; Shi, L. Thermal and structural characterizations of individual single-, double-, and multi-walled carbon nanotubes. *Adv. Funct. Mater.* **2009**, *19* (24), 3918–3925.

(26) Maugis, D. Adhesion of spheres: the JKR-DMT transition using a Dugdale model. *J. Colloid Interface Sci.* **1992**, *150* (1), 243–269.

(27) Zhang, H.; Chen, X.; Jho, Y. D.; Minnich, A. J. Temperature-dependent mean free path spectra of thermal phonons along the c-axis of graphite. *Nano Lett.* **2016**, *16* (3), 1643–1649.

(28) Fu, Q.; Yang, J.; Chen, Y.; Li, D.; Xu, D. Experimental evidence of very long intrinsic phonon mean free path along the c-axis of graphite. *Appl. Phys. Lett.* **2015**, *106* (3), No. 031905.

(29) Sood, A.; Xiong, F.; Chen, S.; Cheaito, R.; Lian, F.; Asheghi, M.; Cui, Y.; Donadio, D.; Goodson, K. E.; Pop, E. Quasi-ballistic thermal transport across MoS₂ thin films. *Nano Lett.* **2019**, *19* (4), 2434–2442.

(30) Liang, Z.; Sasikumar, K.; Koblinski, P. Thermal transport across a substrate–thin-film interface: effects of film thickness and surface roughness. *Phys. Rev. Lett.* **2014**, *113* (6), No. 065901.

(31) Shen, M.; Schelling, P. K.; Koblinski, P. Heat transfer mechanism across few-layer graphene by molecular dynamics. *Phys. Rev. B: Condens. Matter Mater. Phys.* **2013**, *88* (4), No. 045444.

(32) Tanaka, T.; Suzuki, H. The thermal diffusivity of pyrolytic graphite at high temperatures. *Carbon* **1972**, *10* (3), 253–257.

- (33) Kresse, G.; Furthmüller, J. Efficiency of ab-initio total energy calculations for metals and semiconductors using a plane-wave basis set. *Comput. Mater. Sci.* **1996**, *6* (1), 15–50.
- (34) Kresse, G.; Joubert, D. From ultrasoft pseudopotentials to the projector augmented-wave method. *Phys. Rev. B: Condens. Matter Mater. Phys.* **1999**, *59* (3), 1758–1775.
- (35) Perdew, J. P.; Burke, K.; Ernzerhof, M. Generalized gradient approximation made simple. *Phys. Rev. Lett.* **1996**, *77* (18), 3865–3868.
- (36) Grimme, S.; Antony, J.; Ehrlich, S.; Krieg, H. A consistent and accurate ab initio parametrization of density functional dispersion correction (DFT-D) for the 94 elements H-Pu. *J. Chem. Phys.* **2010**, *132* (15), 154104.
- (37) Li, W.; Carrete, J.; Katcho, N. A.; Mingo, N. ShengBTE: A solver of the Boltzmann transport equation for phonons. *Comput. Phys. Commun.* **2014**, *185* (6), 1747–1758.
- (38) Fitzgerald, M. L.; Zhao, Y.; Pan, Z.; Yang, L.; Lin, S.; Sauti, G.; Li, D. Contact Thermal Resistance between Silver Nanowires with Poly (vinylpyrrolidone) Interlayers. *Nano Lett.* **2021**, *21* (10), 4388–4393.
- (39) Yang, J.; Yang, Y.; Waltermire, S. W.; Wu, X.; Zhang, H.; Gutu, T.; Jiang, Y.; Chen, Y.; Zinn, A. A.; Prasher, R.; Xu, T. T.; Li, D. Enhanced and switchable nanoscale thermal conduction due to van der Waals interfaces. *Nat. Nanotechnol.* **2012**, *7* (2), 91–95.
- (40) Pashayi, K.; Fard, H. R.; Lai, F.; Iruvanti, S.; Plawsky, J.; Borca-Tasciuc, T. High thermal conductivity epoxy-silver composites based on self-constructed nanostructured metallic networks. *J. Appl. Phys.* **2012**, *111* (10), 104310.
- (41) Yorifuji, D.; Ando, S. Enhanced thermal conductivity over percolation threshold in polyimide blend films containing ZnO nanoparticle particles: advantage of vertical double percolation structure. *J. Mater. Chem.* **2011**, *21* (12), 4402–4407.
- (42) Xu, J.; Munari, A.; Dalton, E.; Mathewson, A.; Razeeb, K. M. Silver nanowire array-polymer composite as thermal interface material. *J. Appl. Phys.* **2009**, *106* (12), 124310.
- (43) Wang, Z.; Chen, M.; Liu, Y.; Duan, H.; Xu, L.; Zhou, L.; Xu, J.; Lei, J.; Li, Z. Nacre-like composite films with high thermal conductivity, flexibility, and solvent stability for thermal management applications. *J. Mater. Chem. C* **2019**, *7* (29), 9018–9024.
- (44) Fu, C.; Li, Q.; Lu, J.; Mateti, S.; Cai, Q.; Zeng, X.; Du, G.; Sun, R.; Chen, Y.; Xu, J.; Wong, C. P. Improving thermal conductivity of polymer composites by reducing interfacial thermal resistance between boron nitride nanotubes. *Compos. Sci. Technol.* **2018**, *165*, 322–330.
- (45) Zhong, H.; Lukes, J. R. Interfacial thermal resistance between carbon nanotubes: molecular dynamics simulations and analytical thermal modeling. *Phys. Rev. B: Condens. Matter Mater. Phys.* **2006**, *74* (12), 125403.
- (46) Foygel, M.; Morris, R. D.; Anez, D.; French, S.; Sobolev, V. L. Theoretical and computational studies of carbon nanotube composites and suspensions: Electrical and thermal conductivity. *Phys. Rev. B: Condens. Matter Mater. Phys.* **2005**, *71* (10), 104201.
- (47) Bonnet, P.; Sireude, D.; Garnier, B.; Chauvet, O. Thermal properties and percolation in carbon nanotube-polymer composites. *Appl. Phys. Lett.* **2007**, *91* (20), 201910.
- (48) Wu, H.; Drzal, L. T. High thermally conductive graphite nanoplatelet/polyetherimide composite by pre-coating: Effect of percolation and particle size. *Polym. Compos.* **2013**, *34* (12), 2148–2153.
- (49) Zhi, C.; Zhang, L.; Bando, Y.; Terao, T.; Tang, C.; Kuwahara, H.; Golberg, D. New crystalline phase induced by boron nitride nanotubes in polyaniline. *J. Phys. Chem. C* **2008**, *112* (45), 17592–17595.
- (50) Zhi, C.; Bando, Y.; Tang, C.; Honda, S.; Sato, K.; Kuwahara, H.; Golberg, D. Characteristics of boron nitride nanotube-polyaniline composites. *Angew. Chem.* **2005**, *117* (48), 8143–8146.
- (51) Velayudham, S.; Lee, C. H.; Xie, M.; Blair, D.; Bauman, N.; Yap, Y. K.; Green, S. A.; Liu, H. Noncovalent Functionalization of Boron Nitride Nanotubes with Poly (p-phenylene-ethynylene)s and Polythiophene. *ACS Appl. Mater. Interfaces* **2010**, *2* (1), 104–110.
- (52) Meng, W.; Huang, Y.; Fu, Y.; Wang, Z.; Zhi, C. Polymer composites of boron nitride nanotubes and nanosheets. *J. Mater. Chem. C* **2014**, *2* (47), 10049–10061.
- (53) Zhang, Q.; Liu, C.; Liu, X.; Liu, J.; Cui, Z.; Zhang, Y.; Yang, L.; Zhao, Y.; Xu, T. T.; Chen, Y.; Wei, J.; Mao, Z.; Li, D. Thermal transport in quasi-1D van der Waals crystal Ta₂Pd₃Se₈ nanowires: size and length dependence. *ACS Nano* **2018**, *12* (3), 2634–2642.
- (54) Zhao, Y.; Fitzgerald, M. L.; Tao, Y.; Pan, Z.; Sauti, G.; Xu, D.; Xu, Y.; Li, D. Electrical and thermal transport through silver nanowires and their contacts: Effects of elastic stiffening. *Nano Lett.* **2020**, *20* (10), 7389–7396.